MNRAS **434,** 966–977 (2013)
Advance Access publication 2013 July 16
doi:10.1093/mnras/stt973

No evidence for intense, cold accretion on to YSOs from measurements of Li in T-Tauri stars

Darryl J. Sergison,[1]★ N. J. Mayne,[1] Tim Naylor,[1] R. D. Jeffries[2] and Cameron P. M. Bell[1]

[1]*School of Physics, University of Exeter, Stocker Road, Exeter EX4 4QL, UK*
[2]*Astrophysics Group, Keele University, Keele, Staffordshire ST5 5BG, UK*

Accepted 2013 June 3. Received 2013 June 3; in original form 2013 March 12

ABSTRACT

We have used medium-resolution spectra to search for evidence that proto-stellar objects accrete at high rates during their early 'assembly phase'. Models predict that depleted lithium and reduced luminosity in T-Tauri stars are key signatures of 'cold' high-rate accretion occurring early in a star's evolution.

We found no evidence in 168 stars in NGC 2264 and the Orion nebula cluster for strong lithium depletion through analysis of veiling-corrected 6708 Å lithium spectral line strengths. This suggests that 'cold' accretion at high rates ($\dot{M} \geq 5 \times 10^{-4}$ M$_\odot$ yr^{-1}) occurs in the assembly phase of fewer than 0.5 per cent of $0.3 \leq M_\star \leq 1.9$ M$_\odot$ stars.

We also find that the dispersion in the strength of the 6708 Å lithium line might imply an age spread that is similar in magnitude to the apparent age spread implied by the luminosity dispersion seen in colour–magnitude diagrams. Evidence for weak lithium depletion (<10 per cent in equivalent width) that is correlated with luminosity is also apparent, but we are unable to determine whether age spreads or accretion at rates less than 5×10^{-4} M$_\odot$ yr^{-1} are responsible.

Key words: stars: pre-main-sequence – open clusters and associations: individual: NGC 1976 – open clusters and associations: individual: NGC 2264.

1 INTRODUCTION

The radius and luminosity of a pre-main-sequence (pre-MS) star are determined by the balance between its Kelvin–Helmholtz (K-H) contraction time-scale and accretion activity. If accretion increases the mass of the star more rapidly than the K-H time-scale allows energy to be radiated, it will displace the star from thermal equilibrium and cause it to exhibit a radius and luminosity that is inconsistent with non-accreting models (Tout, Livio & Bonnell 1999; Baraffe, Chabrier & Gallardo 2009; Hartmann, Zhu & Calvet 2011). As the age of a T-Tauri star (∼2–5 Myr) can be less than the K-H time-scale, its radius and luminosity may still exhibit the influence of its prior accretion history in the embedded phase.

The core conditions of an embedded proto-star are potentially dependent on its mass accretion rate. Accretion of material with low internal energy ('cold' accretion), at rates in excess of $\dot{M} \geq 10^{-4}$ M$_\odot$ yr^{-1} may gravitationally compress the star, increasing its core temperature and triggering the early onset of lithium burning (Baraffe & Chabrier 2010). Efficient large-scale convection (seen in pre-MS stars) would then rapidly deplete lithium throughout the star. Observationally, this mechanism may be apparent in the later T-Tauri phase as a surface lithium abundance that is much lower than that expected for a given age. In order for lithium to be depleted, a star must be radially compressed and hence the luminosity must be affected. As a result, lithium abundance in combination with luminosity may be a powerful observational signature of heavy accretion during the early evolution of pre-MS stars.

Current support for past accretion at high rates in early stellar evolution stems from three key observations.

(i) Kenyon et al. (1990) find observational evidence for accretion at high rates contributing a significant fraction of a star's mass during the early 'assembly phase' of star formation. Angular momentum conservation indicates that infall must proceed first on to a circumstellar disc. Some of this material may then fall on to the star in bursts, perhaps through gravitational instability. Models by Vorobyov & Basu (2005) predict heavy bouts ($\dot{M} \geq 10^{-4}$ M$_\odot$ yr^{-1}) of accretion lasting ≤100 years, between quiescent periods ($\dot{M} \leq 10^{-6}$ M$_\odot$ yr^{-1}) lasting 1–3 kyr. These time-scales fit with current observations of YSOs, explaining both the large population of low-luminosity class I sources and the small fraction of very luminous sources (Enoch et al. 2009).

(ii) Many observations of both star-forming regions (see Elmegreen 2000, for a review) and local molecular clouds (Ballesteros-Paredes & Hartmann 2007) appear to support the idea

★E-mail: darryl@astro.ex.ac.uk

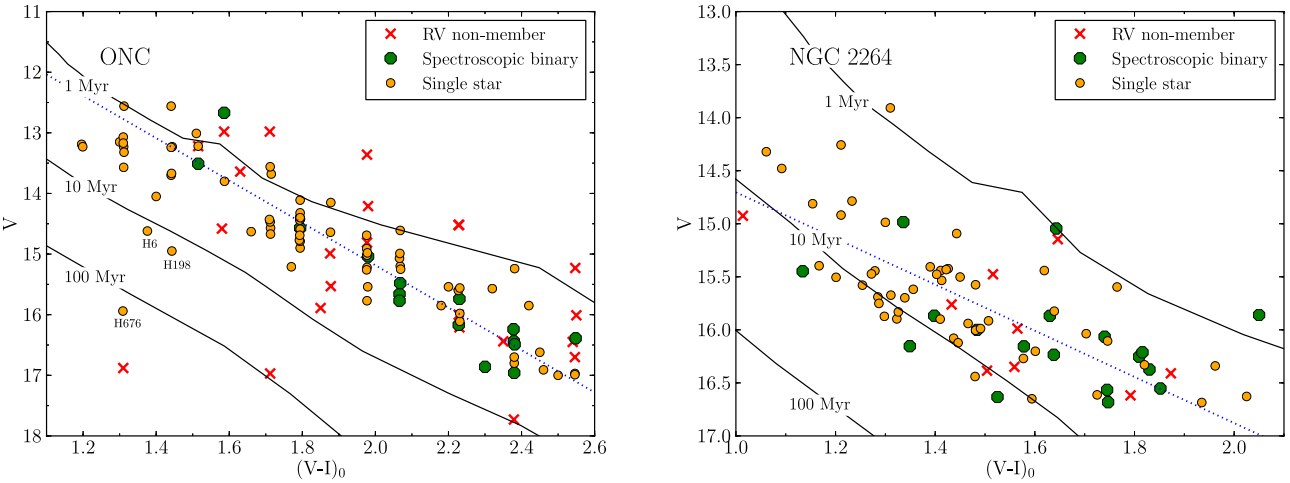

Figure 1. Colour–magnitude diagrams of target cluster members in the Orion nebula cluster (left) and NGC 2264 (right) compared with isochrones from Siess, Dufour & Forestini (2000). Medium orange (light grey) filled circles are confirmed single star members for which we have established veiling and EW[Li]. The large green (dark grey) filled circles are spectroscopic binary stars (and confirmed members) for which we have EW[Li] lower limits. The red crosses depict stars that we observed but were identified as RV non-members. The limits of the plot represent the photometric limits imposed on our sample by (i) the sensitivity of the observations (ii) the $T_{\rm eff}$ cuts applied for the mass range of interest. The dotted (blue) line indicates the division between bright and faint samples defined in Section 5.2. Note: the three members that appear fainter than the 10 Myr isochrone in the ONC are numbered, these are discussed in Section 5.5. ONC photometry from Hillenbrand (1997), NGC 2264 photometry from Mayne et al. (2007).

that star formation occurs of the order of one to a few dynamical crossing times, which is no more than a few Myr for a cluster such as the Orion nebula cluster (ONC) (e.g. Tan, Krumholz & McKee 2006; Jeffries et al. 2011). If this is true then the colour–magnitude diagram (CMD) luminosity dispersion observed in young clusters (see Fig. 1 and McNamara 1976; Palla & Stahler 2000; Da Rio, Gouliermis & Gennaro 2010), that is sometimes attributed to an age spread $\geq$10 Myr, may simply be evidence of variation in radius (and potentially early accretion history) within a coeval population (Jeffries 2007).

(iii) Stars that are unusually depleted in lithium have been reported in the young clusters σ Ori and the ONC (Palla et al. 2005, 2007; Sacco et al. 2007). Some of these lithium-depleted objects are also faint compared with the main cluster population. These characteristics are explained by invoking ages that are at least 10 Myr older than the main cluster population. However, past accretion at high rates may also be a consistent explanation and does not need to invoke an age spread that is at odds with observations of star formation on a dynamical crossing time.

Accreting material adds gravitational and thermal energy to the stellar interior at a rate defined by Hartmann, Cassen & Kenyon (1997) as

$$\frac{{\rm d}E_{\rm acc}}{{\rm d}t} = \alpha\,\epsilon\,\frac{G\,M_\star\,\dot{M}}{R_\star}, \qquad (1)$$

where $\epsilon \leq 1$ for material falling from within the star's potential well and $\epsilon \leq 0.5$ for material accreted through a boundary layer from a thin disc. α is the fraction of the accretion luminosity absorbed by the star. Hartmann et al. (1997) suggest that $\alpha \ll 1$, providing the fraction of the stellar surface that accretion occurs over is small.

These qualitative ideas are backed by the results of numerical simulations, such as those by Tout et al. (1999), Baraffe et al. (2009), Baraffe & Chabrier (2010), Hosokawa, Offner & Krumholz (2011) and Baraffe, Vorobyov & Chabrier (2012). Baraffe & Chabrier (2010) find that in the limit where $\alpha \lesssim 0.2$ (termed 'cold' accretion) additional mass added to the star causes gravitational contraction, reducing overall luminosity and increasing core temperature and pressure. They also find that this process significantly depletes lithium abundance in very young stars (from $\lesssim$1 Myr) with $M_\star < 2\,{\rm M}_\odot$. The models suggest that a threshold accretion rate exists whereby detectable lithium depletion occurs if the accretion rate during bursts exceeds $\dot{M} \geq 5 \times 10^{-4}\,{\rm M}_\odot\,{\rm yr}^{-1}$ and the initial core mass of the proto-star has a mass $\leq$0.03 $\rm M_\odot$ (see Fig. 2). For a 1 $\rm M_\odot$ star, cold accretion that is able to measurably change a star's luminosity is found to always cause a measurable depletion in lithium.

Lithium depletion occurs as the abundance of lithium in the photosphere is a sensitive function of the temperature at the core of a fully convective star. Once temperatures exceed $\sim 2.5 \times 10^6$ K (slightly below that required for hydrogen burning), lithium is swiftly depleted via $^7{\rm Li} + {\rm p} \rightarrow {}^4{\rm He} + \alpha$ reactions.

In contrast, non-accreting models suggest that lithium depletion will occur much later in the star's evolution. Siess et al. (2000) and Baraffe et al. (2002) predict less than 20 per cent lithium depletion for stars of age <10 Myr at masses above 0.6 $\rm M_\odot$.

Cold accretion models make two clear predictions which we test by observation.

(i) If accretion occurs at $\dot{M} \geq 5 \times 10^{-4}\,{\rm M}_\odot\,{\rm yr}^{-1}$, some highly lithium-depleted stars should be found that cannot be explained by non-accreting evolutionary models.

(ii) In the cold accretion model, lithium depletion and low-luminosity result from the same mechanism, hence observed lithium depletion should correlate with the appearance of old age in the CMD.

Section 2 describes the theoretical models and the observation target selection. Section 3 details our observations and data reduction process. Section 4 presents our results, including radial velocity (RV), binarity, accretion veiling, $v \sin i$ and lithium equivalent width. In Section 5, we discuss the lithium and veiling results for each cluster and show that there is some correlation between lithium abundance and CMD position. In Section 6, we conclude that there is no evidence for past episodes of cold accretion at very high rates.

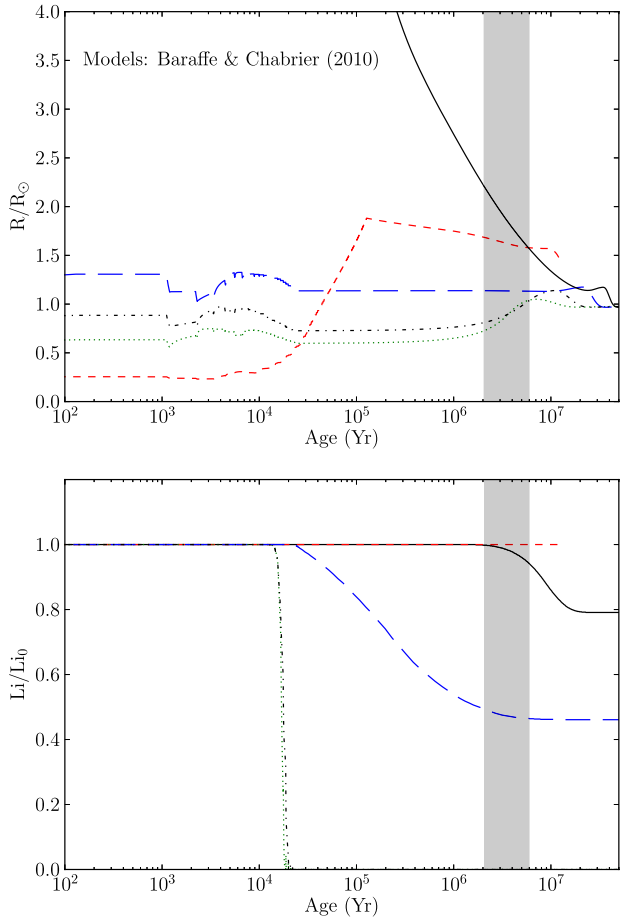

Figure 2. Evolution of radius (upper panel) and photospheric lithium abundance (lower panel) as a function of time for Baraffe & Chabrier (2010) models with episodic accretion and reaching a final mass of $1\,M_{\odot}$. Short dash (red): $M_{\rm init} = 1\,M_{\rm jup}$, $\dot{M}_{\rm burst} = 1 \times 10^{-4}\,M_{\odot}\,{\rm yr}^{-1}$, $N_{\rm burst} = 100$; dot (green): $M_{\rm init} = 10\,M_{\rm jup}$, $\dot{M}_{\rm burst} = 5 \times 10^{-4}\,M_{\odot}\,{\rm yr}^{-1}$, $N_{\rm burst} = 20$; dash–dot (black): $M_{\rm init} = 20\,M_{\rm jup}$, $\dot{M}_{\rm burst} = 5 \times 10^{-4}\,M_{\odot}\,{\rm yr}^{-1}$, $N_{\rm burst} = 20$; long dash (blue): $M_{\rm init} = 30\,M_{\rm jup}$, $\dot{M}_{\rm burst} = 5 \times 10^{-4}\,M_{\odot}\,{\rm yr}^{-1}$, $N_{\rm burst} = 20$; solid line (black) is a non-accreting model for a $1\,M_{\odot}$ star. All calculations are made with $\Delta t_{\rm burst} = 100$ yr and $\Delta t_{\rm quiet} = 1000$ yr. The grey shaded region encompasses age estimates for the clusters studied in this paper.

2 THEORY AND TARGET SELECTION

2.1 Theoretical lithium depletion

Fig. 3 shows simulated lithium isochrones based on several different interior models (Siess et al. 2000; Baraffe et al. 2002) and illustrates the predicted equivalent width of the 6708 Å lithium line (EW[Li]) as a function of $(V - I_{\rm c})_0$ colour. The isochrones were derived using a colour – $T_{\rm eff}$ relation defined by observations of main-sequence stars (Kenyon & Hartmann 1995), curves of growth from Jeffries et al. (2003) and an assumed initial lithium abundance of A(Li) = 3.3 on the logarithmic scale of Anders & Grevesse (1989). Comparison of the isochrones with those created using a Pleiades tuned colour–$T_{\rm eff}$ relation (from Jeffries & Oliveira 2005) show that whilst the colour bounds of the lithium depletion 'chasm' vary as a function of model, the location of the isochrones do not vary by more than ±0.1 in $(V - I_{\rm c})_0$.

These models suggest that lithium depletion can be used as a sensitive indicator of age in the mass range $0.4 < M_{\star} < 0.6\,M_{\odot}$ ($3400 < T_{\rm eff} < 3800$ K, $1.2 < (V - I_{\rm c})_0 < 2.6$). Outside this range, pre-MS stars of lower mass than $0.4\,M_{\odot}$ reach the temperature for lithium burning too slowly to show depletion in young (<10 Myr) clusters. Stars of mass $>0.6\,M_{\odot}$ develop a radiative core early and the base of the convective zone rises to regions of cooler temperature before all lithium can be destroyed (Pinsonneault 1997), rendering lithium depletion ineffective as an age indicator in young clusters.

Studies by Palla et al. (2005), Palla et al. (2007) and Sacco et al. (2007) derive ages based on EW[Li] for individual stars in the ONC and σ Ori. They compare lithium depletion ages for each star with that found using isochrone fitting in the CMD. A small number of objects are identified in each cluster with anomalously low lithium line strength and in a few cases these correlate with an older CMD age. The lithium-derived age spread found within the clusters is proposed to support a slow star formation model. However, a small number of stars in the very low mass regime ($\lesssim 0.25\,M_{\odot}$) are found in both the ONC and σ Ori with lithium depletion significantly greater than that expected from their CMD age.

Lithium depletion predicted from simulations of cold accretion may occur throughout the mass range (see examples in Baraffe & Chabrier 2010, of stars with mass 0.1 and $1\,M_{\odot}$) providing the mass accretion rate during bursts $\dot{M} \geq 5 \times 10^{-4}\,M_{\odot}\,{\rm yr}^{-1}$. Conversely, age related depletion is highly sensitive to mass and is

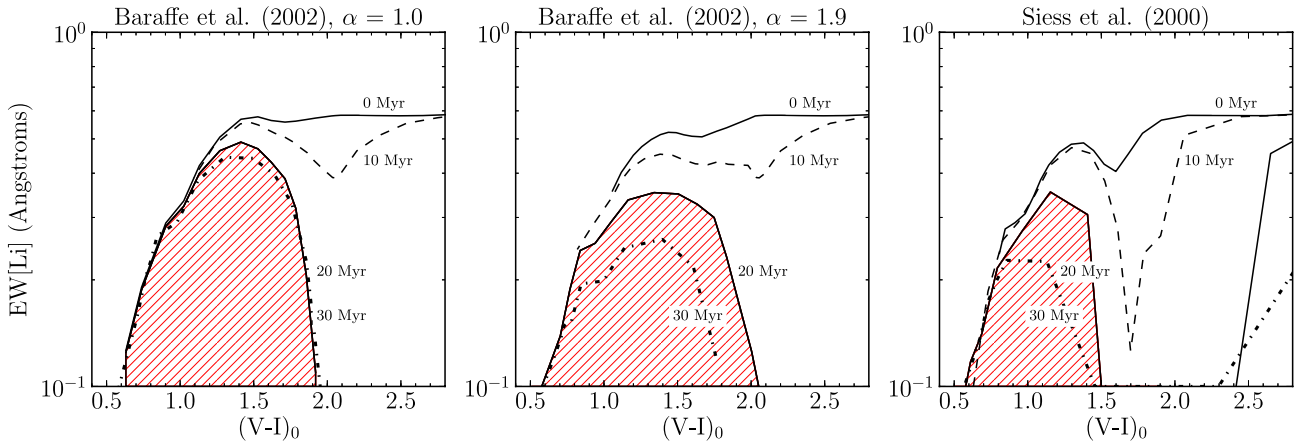

Figure 3. Predicted evolution of the 6708 Å lithium line strength as a function of age and colour in non-accreting models of pre-MS stars. The (red) hatched region is where we expect to find no stars that are younger than 20 Myr, thus defining a 'forbidden zone' in our clusters based on current age estimates. Stellar interior models are from Baraffe et al. (2002) and Siess et al. (2000), $T_{\rm eff}$ to $(V - I_{\rm c})_0$ from Kenyon & Hartmann (1995), curves of growth from Jeffries et al. (2003), A(Li) = 3.3 from Anders & Grevesse (1989).

Table 1. Key parameters for clusters selected in this study.

Cluster	Age (Myr)	Distance modulus	Number of selected targets	Supporting catalogues
Orion nebula cluster	2[(a)]	8.08±0.04[(b)]	115	Hillenbrand (1997)
NGC 2264	3[(a)]	$9.37^{+0.15}_{-0.11}$ [(a)]	88	Mayne et al. (2007)

[a] Mayne & Naylor (2008)
[b] Menten et al. (2007)

shown by some stellar interior models to be suppressed in the range 0.6–2 $M_\odot$ due to the onset of the radiative core. As a result, the region in EW[Li] versus colour space within the range $0.5 > (V - I_c)_0 > 1.6$ and below an EW[Li] of 0.35 Å is a 'forbidden zone' (shown in Fig. 3), where low lithium objects should not exist according to non-accreting models. Confirmed young cluster members found in the forbidden zone would offer strong support to cold accretion theories, even if combined with modest age spreads.

2.2 Target selection

The constraints established in Section 2.1 lead us to require nearby young clusters with ages <10 Myr, where lithium depletion may identify pre-MS members with a high accretion rate history or greater age. We also required comprehensive literature photometry and spectroscopy to characterize the observed stars and allow construction of CMDs for isochronal age determination. The clusters selected were the ONC and NGC 2264. Key parameters for these clusters are shown in Table 1. Whilst previous age estimates for these clusters are around 2–3 Myr, recent work by Naylor (2009) and Bell et al. (2013) suggest that pre-MS ages are underestimated by a factor of 2, hence our clusters may in reality be closer to 4–6 Myr.

To ensure a high fraction of stars studied were cluster members, indicators of youth such as X-ray luminosity (Flaccomio et al. 1999, 2002), Hα emission (Dahm & Simon 2005) and optical variability (Herbst et al. 2002; Lamm et al. 2004) were used in conjunction with position in colour–magnitude space to select target stars. Importantly, photometric selection did not exclude members with low luminosity. Instrumental constraints meant that selection was also weighted towards the cluster centre, thus preferring a smaller number of objects close to the cluster core over a larger number further out. This led to the selection of fewer stars per field, although those selected had a higher probability of cluster membership. The final selection criteria for target stars was a cut in $T_{\rm eff}$ (determined via the colour–$T_{\rm eff}$ relation of Kenyon & Hartmann 1995) in the range 3400–4900 K, approximately corresponding to mass range 0.3–1.9 $M_\odot$ on the isochrones of Siess et al. (2000) at an age of 3 Myr.

For the ONC, the selection deliberately targeted seven literature cluster members that appear to be fainter than the main population in the CMD. Since low-luminosity objects could result from cold accretion, we shall investigate whether these objects also exhibit depleted lithium. Alternative theories proposed to explain them include an age spread (Palla & Stahler 2000), as gravitationally captured field stars (Pflamm-Altenburg & Kroupa 2007) or unusually blue objects exhibiting heavy accretion veiling (Hillenbrand 1997). We shall refer to this population in the rest of the paper as the 'low-luminosity group' (LLG).

3 OBSERVATIONS AND DATA REDUCTION

The observations were made on the nights of 2011 November 20, 21 using the AF2/WYFFOS multi-object fibre-fed spectrograph on the 4.2 m *William Herschel* Telescope. The small fibres module contains 150 fibres, each with a diameter of 1.6 arcsec. To avoid potentially damaging fibre collisions, not all of the fibres may be placed on target stars in any given configuration, thus limiting the actual number of targets to significantly less than 150 per field. This was an important limiting factor in these observations due to the centrally condensed nature of the clusters studied. We used an echelle grating and order sorting filter, centred at 6545 Å with a range of ∼390 Å. This covered the wavelength range including Hα and the lithium doublet at 6708 Å. The signal-to-noise (SNR) obtained ranged from 10–60 per 0.22 Å wavelength step with a resolution, $R \sim 10\,000$.

Fibre setups were configured to maximize the number of cluster members observed. Time, weather and observability constraints meant that for the ONC two 'bright' (1 × 2700 s) and one 'faint' (4 × 2700 s) setups were obtained and for NGC 2264 three 'bright' (1 × 2700 s) setups. The longer exposure times for the ONC were offset by the greater levels of extinction to that cluster ($A_v \sim 1.5$–6, Hillenbrand 1997) as compared with NGC 2264 ($A_v = 0.37$, Mayne et al. 2007). As a result, the limiting magnitude (corrected for extinction) for both clusters was $V_0 \geq 17$. 115 stars were observed in the ONC and 88 in NGC 2264.

Science frames were bias corrected using a median of five bias frames, with bad pixels identified from dark frames and subsequently masked. Tungsten lamp flat-fields were obtained before each science exposure and used to trace the positions of spectra on the CCDs. Flat-field images were also used to construct a weighting function for the optimal extraction routine. Arc lamp exposures before and after each science frame were used to provide wavelength calibration. Sky signal was subtracted using a minimum of 30 randomly placed sky fibres. The spectra were extracted and calibrated using an IDL-based software pipeline provided by the *Issac Newton* Group and optimized for the AF2/WYFFOS instrument.[1] Spectra were extracted using an optimal routine (see Horne 1986) which helps to minimize statistical noise. Once calibration and reduction were complete the data were then interpolated and re-binned on to 10 000 logarithmically placed wavelength steps.

Target spectra, measured relative RVs, lithium equivalent widths and veiling fractions in this paper are freely available from the Cluster Collaboration home page[2] and the CDS archive (a sample may be seen in Table 2).

[1] http://www.ing.iac.es/astronomy/instruments/af2/reduction.html
[2] http://www.astro.ex.ac.uk/people/timn/Catalogues/

Table 2. Summary of derived parameters from this study. Table 2 is published in its entirety in the electronic edition. A portion is shown here for guidance regarding its form and content. Coordinates are RA, Dec. (J2000.0). Importantly, the resolution and sky subtraction scheme used in this analysis mean that nebular line contamination of Hα measurements is likely to be significant and thus Hα data should be used with caution. EW[Hα] measurements are not corrected for veiling.

RA (hh mm ss.ss)	Dec. (dd mm ss.ss)	EW[Li] (Å)	ΔEW[Li] (Å)	RV (km s^{-1})	ΔRV (km s^{-1})	r_j –	Δr_j –	EW[Hα] (Å)	ΔEW[Hα] (Å)	vel Hα (km s^{-1})	Δvel Hα (km s)$^{-1}$
05 35 16.32	−05 15 38.00	0.667	0.039	0.5	2.8	0.29	0.04	−45.50	0.03	71.76	1.83
05 35 04.20	−05 15 21.44	0.596	0.046	4.8	2.8	0.59	0.10	−142.01	0.08	80.90	1.83
05 34 52.25	−05 12 03.20	0.625	0.051	−3.8	2.8	0.14	0.04	−32.50	0.05	84.56	1.83

4 ANALYSIS

The 6708 Å lithium line equivalent width (EW[Li]) was measured with respect to a pseudo-continuum. A wavelength step integration of the spectral line was performed between upper and lower line limits defined to exclude other lines and to incorporate the entire line irrespective of rotational broadening or binarity. At the resolution of our spectra, contamination of up to 20 mÅ is likely to be present from a weak Fe I line at 6707.4 Å. Uncertainty on definition of the pseudo-continuum and line limits were determined through repeat measurements to be ±10 mÅ. Photon noise in the signal contributes a further ±10–60 mÅ, dependent on the SNR of the spectrum. The three uncertainties are combined in quadrature with that described in Section 4.2 for accretion veiling.

As we are trying to measure the intrinsic EW[Li] for these stars, we must account for 'veiling' of spectral lines by continuum emission from magnetospheric accretion regions on the surface of the star. This 'veiling' effect is well studied (e.g. Gahm et al. 2008; Dodin & Lamzin 2012) and its effect has been corrected through the use of techniques outlined in Hartigan et al. (1989). The accretion veiling contamination is visible as a weakening of absorption lines and hence has a significant effect on the measurement of photospheric features such as the 6708 Å lithium line. The effect of accretion veiling is to reduce measured EWs, hence without careful consideration this could affect the apparent lithium abundance in the objects being studied. A correction for the veiling flux is made assuming that it is a smoothly varying continuum over the spectral range from 6390 to 6710 Å. Within the narrow range specified this is a reasonable assumption as determined by Hartigan et al. (1989) and Guenther & Hessman (1994). Before determining and correcting for veiling, an assessment of RV and $v \sin i$ must first be made between the object and template stars in order to correct for wavelength and line profile differences. Typically the unveiling process contributes an uncertainty of similar magnitude to the combined measurement uncertainties and is combined with them to provide an uncertainty estimate on the final measurements.

4.1 Radial velocity and binary stars

RVs were determined using cross-correlation of spectral lines in the range 6385−6510 Å between each star and an arbitrary (low $v \sin i$) single star reference in the field. No absolute RV standards were measured as relative velocities are sufficient for veiling analysis and cluster membership verification. Fig. 4 shows histograms of the derived RV distributions for both clusters.

The ONC displays a clear velocity grouping with a range of ±10 km s^{-1} about the sample median, this is consistent with previous RV studies of this cluster (e.g. Biazzo et al. 2009). 21 objects were identified with velocities outside the range specified and hence were removed from further analysis of the sample. Many of these objects are likely to be unequal mass spectroscopic binary cluster members that are unresolved from their cross-correlation function (CCF); however, without multi-epoch measurements we cannot be clear as to which objects fall into this category. As a result we reject all stars with |RV| > 10 km s^{-1}.

The NGC 2264 RV histogram shows that this cluster exhibits a non-Gaussian velocity dispersion with a range of ±9 km s^{-1}

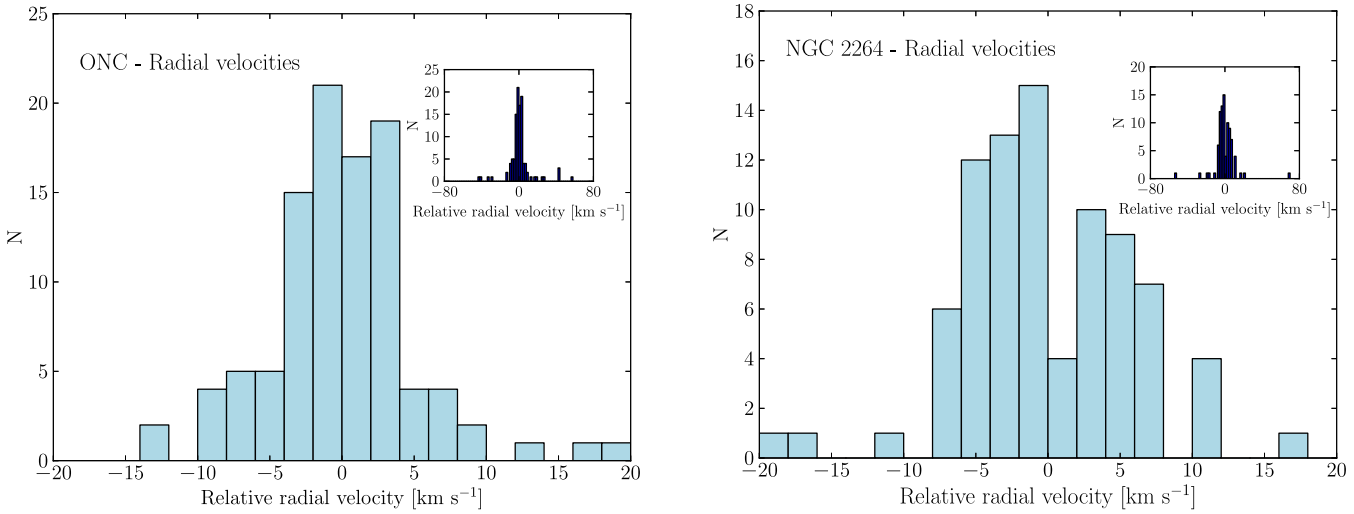

Figure 4. Histogram of RVs for stars in the ONC (left) and NGC 2264 (right) relative to the median of the respective samples. Inset shows the entire sample including RV outliers.

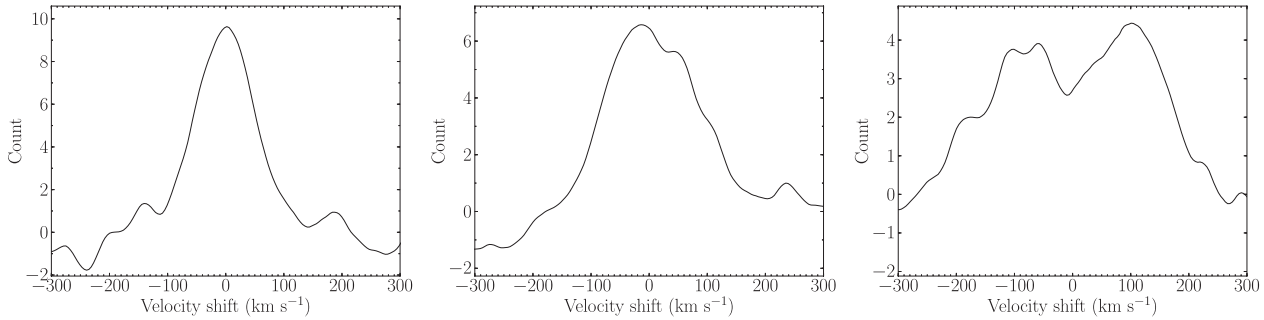

Figure 5. Example velocity CCF plots, showing single star (left), and close and wide line separation binary stars (centre and right).

about the median. This is consistent with previous measurements by Fűrész et al. (2006). Nine objects in the NGC 2264 sample exhibit RV with magnitudes outside the range defined above and hence have also been removed from further analysis.

Some of the identified RV outliers exhibit lithium absorption and Hα emission, so are likely to actually be cluster members. We have been deliberately cautious in excluding potential non-members though, as our aim was to set up a robust sample of members that does not use lithium detection as a criterion. Exclusion of some stars which are actually members only affects the result by reducing the sample size. Conversely, including a star that was not a member could seriously bias the result.

Binary stars with resolved splitting in spectral lines cause significant difficulties with accretion spectrum fitting. Potential binaries were identified since they exhibit multiple peaks in the CCF and were removed from the data set before the veiling analysis. Examples showing single and binary star CCFs are shown in Fig. 5. Multiple peaks in a broad CCF could also be due to noise overlaid on highly rotationally broadened spectra. This is difficult to confirm or refute on a star by star basis; however, unveiled Li[EW] measurements for these stars were included in the analysis as veiled lower limits in EW[Li].

Four of the seven stars in the ONC 'LLG' (see Section 2.2) were identified as having RVs that are inconsistent with the cluster. As a result they are removed from the sample and their faint nature may be explained as being characteristic of main-sequence or post-main-sequence stars from the Galactic field that are moving through or behind the cluster. These objects are illustrated by red crosses in Fig. 1.

4.2 Accretion veiling and $v \sin i$

The magnitude of veiling for a given object over wavelength range j is expressed as

$$r_j = \frac{k_j}{S_{\rm phot}}, \qquad (2)$$

where r_j is the flux ratio of the accretion veiling continuum (k_j) to the stellar photospheric continuum ($S_{\rm phot}$).

To estimate the veiling continuum flux, a set of template stars have been selected for each cluster from their own populations (nine for the ONC and eight for NGC 2264) across the full colour range. Selected template stars form the upper envelope of the EW[Li] versus $(V-I_{\rm c})_0$ diagram and exhibit $v \sin i$ limited by instrument full width at half-maximum (FWHM). Hence these objects should be amongst those with the lowest veiling and intrinsic $v \sin i$ within our sample. The templates were first offset in wavelength to compensate for the difference in RV between template and object. They were

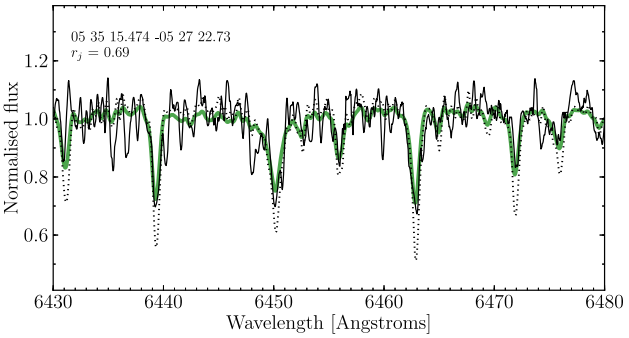

Figure 6. Spectrum of object RA = 05$^{\rm h}$ 35$^{\rm m}$15$^{\rm s}$.47 Dec. = −05° 27′ 22″.7 in the ONC. The thin black line is the object spectrum. The dotted line is the template showing significantly deeper photospheric absorption lines. The green (light grey) broad line is the broadened and veiled template that best fits the object spectrum ($r_j = 0.69$).

then rotationally broadened (using a kernel with limb darkening coefficient of 0.5; van Hamme 1993) and normalized to a similar flux as that of the object spectrum to produce reference templates.

The templates were then subtracted from the object spectrum to leave residuals which are assumed to represent the accretion spectrum. We varied the normalization of the templates and examined the residuals using a χ^2 test, performed between the residuals and (30 Å boxcar average) smoothed versions of themselves. Adopted $v \sin i$ and veiling values were identified using the residuals with minimum χ^2. The parameter search space was defined by $v \sin i$, from 0–100 km s^{-1} with a resolution of 1 km s^{-1} and veiling ratio of 0–5 in steps of 0.01 of the photospheric continuum. Fig. 6 shows an example of an object spectrum, template and best-fitting broadened and veiled model template.

This process was repeated as it was found that a considerably stronger CCF was obtained if the RV cross-correlation is performed against an appropriately broadened template. Thus, the first iteration identifies approximate RV and $v \sin i$, the second iteration improves the RV and hence $v \sin i$ as the fitted RV template has a more similar shaped line profile.

Fitting of templates was performed in two wavelength regions, the first between 6390 and 6500 Å, in a region containing seven photospheric absorption lines (Fe I 6393.6 Å, Ne II 6407.9 Å, Fe I 6411.7 Å, Fe I 6421.3 Å, Fe I 6431.0 Å, Ca I 6439.1 Å, Ca I 6450.0 Å, Ca I 6462.5 Å and Fe I 6495 Å). The second was between 6610 and 6675 Å, containing three lines (V I 6624.8 Å, Ni I 6643.6 Å and Fe I 6663.4 Å). These regions are free from contamination by Hα or significant sky and nebular line emission.

Analysis of sky and nebular lines indicate that the spectrograph was operating with a resolution of $R \sim 10\,000$. Comparison with

literature (see Rhode, Herbst & Mathieu 2001; Baxter et al. 2009) indicate that our limit in $v \sin i$ resolution is ∼20–30 km s^{-1}, depending on target SNR.

The veiling for each star was calculated as the weighted mean across the cluster template set based on the inverse of the difference in $(V - I_c)_0$ colour between each template star and the object. To avoid overweighting when the template and object colours were very close, a minimum $\Delta(V - I_c)_0$ of 0.1 was placed on the weighting algorithm. The aim of this process is to use multiple templates to provide reliability of fit, without introducing errors from large template-to-star colour differences. It should be noted that despite the efforts taken to ensure that the veiling was derived from templates of similar colour, in practice the veiling measured was found to be surprisingly insensitive to template colour for any given star. The range of fractional uncertainty due to template mismatch was measured to be ∼0.05–0.3 across our sample. Template to template variations appear to dominate, possibly caused by differences in the template line profiles due to rotation, binarity and chromospheric activity.

Uncertainties in veiling were derived by analysing the range in veiling estimates returned by all of the fits from the full template set. The standard deviation (also weighted as a function of template to star colour difference) of the set of veiling values was calculated and adopted as the uncertainty in the veiling measurement.

As the method used here analyses lines over a narrow spectral range, it is independent of reddening and extinction and hence is robust in dusty regions of new star formation such as the clusters studied in this paper. Measured values of r_j vary from 0 to 4.0.

4.3 Lithium equivalent width versus colour

Once the magnitude of the veiling continuum had been established for each star, a correction was applied to the raw measured lithium EW to quantify the unveiled EW. The uncertainty in the corrected EW[Li] was calculated by combining uncertainties in the raw line measurements with the uncertainty in veiling. Fig. 7 shows veiling corrected lithium EWs and associated uncertainties plotted as a function of dereddened $(V - I_c)_0$ colour. Most of our data points lie slightly above the undepleted model isochrone. Reasons for this may include uncertainties in molecular line strengths in stars with $T_{\rm eff} <$ 4000 K, causing difficulty in definition of the pseudo-continuum around the lithium line. In the hotter stars, a lack of inclusion of non-linear thermodynamic effects may cause uncertainties in the modelled curves of growth (e.g. Carlsson et al. 1994). Theoretical 0 (undepleted), 10 and 20 Myr isochrones (Baraffe et al. 2002) are also shown. Dereddened $(V - I_c)_0$ colours for the ONC are from Hillenbrand (1997). It should be noted that the dereddening method used for the ONC was performed on a star-by-star basis and groups objects into bins by spectral class. Hence $(V - I_c)_0$ colours are not continuous. Dereddened colours for NGC 2264 were derived in Mayne et al. (2007) using a single global solution of $E(V - I_c) =$ 0.15, based on a mean measured $(V - I_c)$ excess for main-sequence stars.

Accurate unveiling of spectroscopic binaries is a very difficult and uncertain process, so these points have been left in their raw measured (veiled) values and are displayed as lower limits in EW[Li].

4.4 Hydrogen α measurements

The spectral range of our data included the Hα line at 6563 Å. Whilst it is beyond the scope of this paper to analyse this feature, measurements of Hα equivalent width and the velocity width at 10 per cent of peak line flux have been measured and are included in the tables of data for future reference. Importantly, the Hα equivalent width measurements presented are not corrected for accretion veiling. Sky and nebular line subtraction for this data set has been performed using a median combination of randomly placed sky fibres and at the resolution of our study, structure within the Hα line is poorly resolved. These two factors mean that nebular line contamination of Hα measurements is likely to be significant (see Fűrész et al. 2008) and thus these data should be used with caution.

Data from this paper are available online as an electronic table. An example of the data format is shown in Table 2. Spectra are also available online for all of our targets.

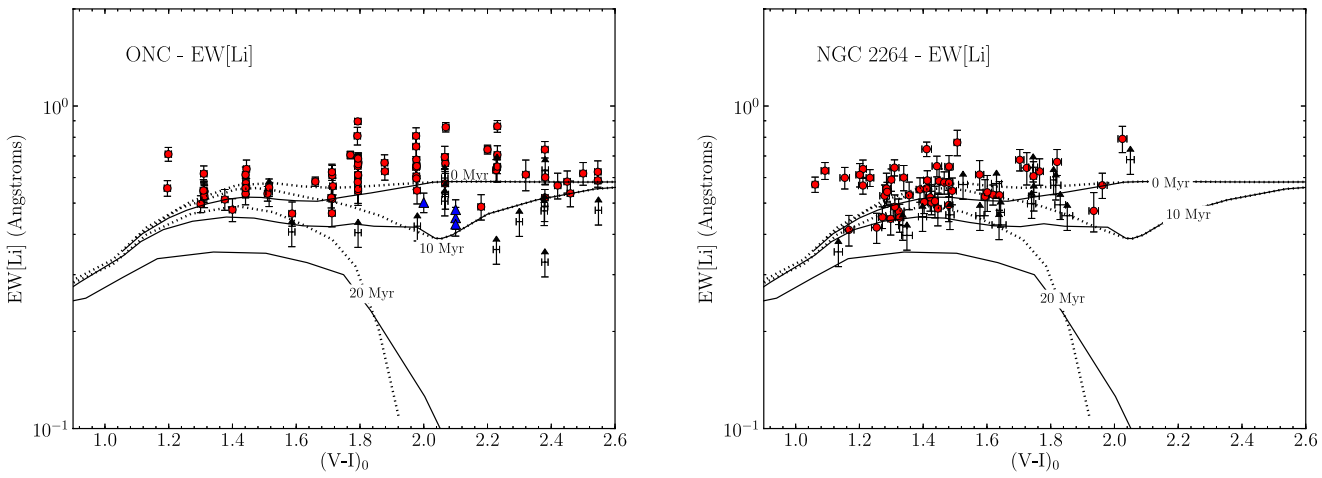

Figure 7. A comparison of 6708 Å lithium line equivalent width measurements for stars in the ONC (left) and NGC 2264 (right) plotted as a function of intrinsic $(V - I_c)_0$. The red points are unveiled single star measurements, black triangles are lower limits for spectroscopic binaries which are left as veiled (raw) measurements. The 0, 10 and 20 Myr isochrones are based on models by Baraffe et al. (2002). The solid lines indicate models using a convective mixing length parameter (α) of 1.9. The dotted lines indicate $\alpha = 1.0$. The blue triangles are data from Palla et al. (2005) which are cited as having depleted lithium. These points have been calculated using n(Li) to EW[Li] conversion from curves of growth in table 1 of Palla et al. (2007). The conversion from $T_{\rm eff}$ to intrinsic $(V - I_c)_0$ colour for the Palla et al. (2005) data have been made using the relation defined by Kenyon & Hartmann (1995).

5 DISCUSSION

5.1 Accretion veiling

Our data show that our sample of stars in the ONC exhibit greater accretion veiling than our sample in NGC 2264. The mean r_j and standard deviation have been calculated for all stars in both clusters and for a subset in both clusters that cover a common colour range ($1.2 < (V - I_c)_o < 2.0$). All measured stars in the ONC exhibit a mean $r_j = 0.48$ with a standard deviation (σ) of 0.68. This compares with mean $r_j = 0.16$, $\sigma = 0.19$ for all measured stars in NGC 2264. The subset with colour range $1.2 < (V - I)_c < 2.0$ in the ONC exhibit a mean $r_j = 0.44$, $\sigma = 0.71$ and in NGC 2264 the mean $r_j = 0.15$, $\sigma = 0.18$. It is notable that whilst the absolute levels of veiling differ, the ratio of σ / r_j is similar in both clusters.

If NGC 2264 is older than the ONC as suggested through studies of young main-sequence stars (Mayne & Naylor 2008) then our finding is consistent with models of decreasing disc fraction (and hence accretion) with age. If however, the ages of the clusters are indistinguishable from each other as suggested by main-sequence turn-off ages (see Naylor 2009) then the difference in apparent accretion luminosity may suggest an environmental difference between the two clusters such that stars in the ONC accrete more vigorously or for longer than NGC 2264.

5.2 Accretion veiling correlation with CMD position

To test for any correlation between veiling and position in the CMD, each cluster was split on to two sub-samples representing the bright and faint populations using the following method. First, we calculated the median dereddened colour in 0.1 mag. wide magnitude bins and a straight line was fitted to define the median magnitude as a function of colour. These lines may be seen plotted over the data in Fig. 1. Stars with magnitudes brighter than this were assigned to the bright sub-sample and vice-versa. Histograms of veiling strength in the two luminosity samples are shown for each cluster in Fig. 8.

We tested the null hypothesis that the bright and faint sub-samples were drawn from the same parent veiling distribution using a two-sample K-S test. For the ONC, the null hypothesis was rejected with 64 per cent confidence that the populations are distinct, with a bright median $r_j = 0.24$ and a faint median $r_j = 0.23$. The implication is that there is no correlation between veiling and CMD position for the ONC.

The null hypothesis was rejected with 98.3 per cent confidence for NGC 2264. This suggests that the brighter stellar population exhibits greater levels of accretion (median bright $r_j = 0.17$, median faint $r_j = 0.09$). The histogram shown in Fig. 8 indicates that this result is mostly driven by just a few veiled objects in the bright population.

5.3 EW[Li] distribution, age spreads and correlation with CMD position

Both clusters appear to exhibit lithium equivalent widths that are approximately consistent with their CMD derived ages (<10 Myr). It is also apparent that no highly lithium-depleted stars are seen with EW[Li] $\lesssim$ 0.4 Å. NGC 2264 appears to show a slightly greater spread in EW[Li] at higher masses than the ONC.

The observed dispersion in EW[Li] might imply an age spread that is similar in magnitude to the apparent age spread implied by the luminosity dispersion seen in CMD space. To test whether this really could be an age spread, we looked for disagreement between the EW[Li] seen in the bright and faint sub-populations defined previously for accretion veiling (see Section 5.2). If an age spread explanation were to be plausible, the bright sample should be the youngest and ages should increase as one moves to fainter magnitudes. This should be evident as a depletion in lithium in the faint population.

We compared the sub-populations for each cluster using the two-sample K-S test. The ONC shows evidence for the two samples being drawn from different populations with the null hypothesis that they are from the same population being rejected at the 99.8 per cent confidence level. The bright population exhibits median EW[Li] = 0.63 Å and the faint population median EW[Li] = 0.56 Å. A similar trend is shown in NGC 2264, the bright population exhibits median EW[Li] = 0.59 Å and the faint population EW[Li] = 0.54 Å with the null hypothesis being rejected at the 98.2 per cent confidence level. These findings are illustrated in Fig. 9.

We have carefully considered whether this trend in EW[Li] is a systematic effect of the unveiling process. Although there is a weak

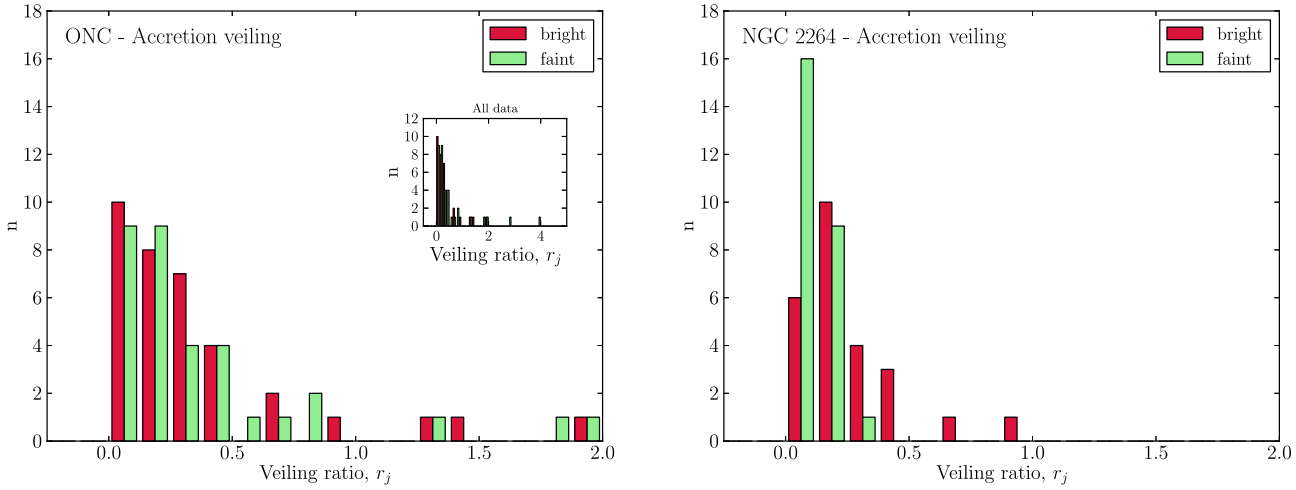

Figure 8. Comparison of accretion veiling ratio r_j as a function of CMD luminosity sample for the ONC (left) and NGC 2264 (right). Each cluster is split into a bright and faint population as described in Section 5.2. Note the axes used for both clusters are the same to aid comparison; however, the ONC exhibits an extended tail of objects at high veiling ratios (shown in the inset plot).

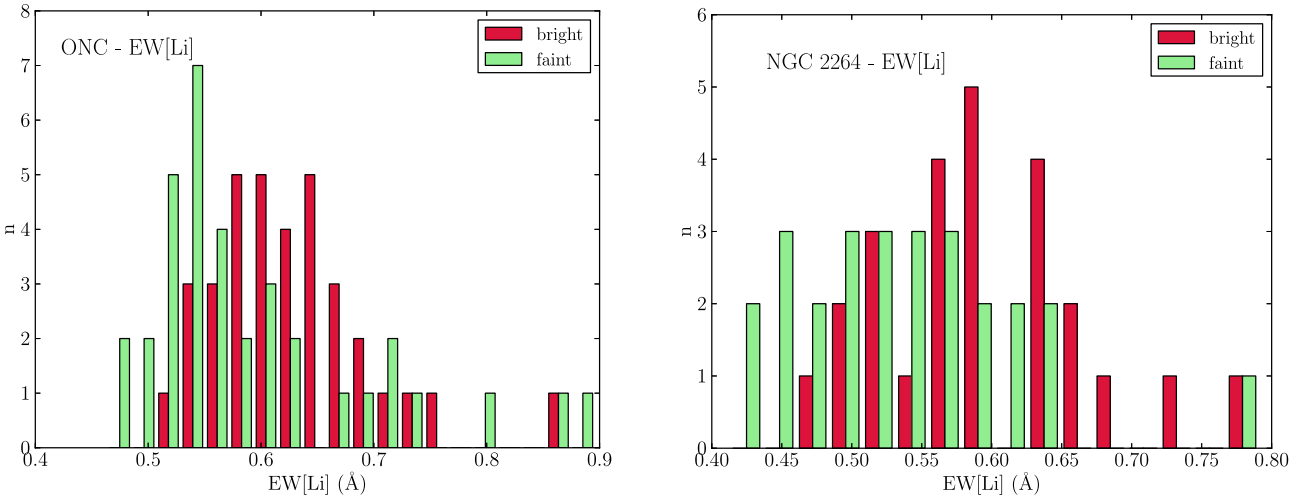

Figure 9. Comparison of the EW[Li] data for bright and faint sub-samples in each cluster. In both clusters the population of faint stars shows a systematic decrease in lithium line strength.

correlation between EW[Li] and veiling, this cannot be the cause of the correlation of CMD position with Li[EW] since there is not the correlation between veiling and position in the CMD which would be required to translate this into the observed effect. It should be noted that if there is a veiling-related systematic error, one would expect its effect to be most apparent in the ONC where veiling is strongest. In practice, the ONC shows no correlation between veiling and CMD position, yet the EW[Li] versus CMD position correlation is significant.

We have also considered whether this trend in EW[Li] may be due to differences in surface gravity; however, the correlation is in the opposite sense to that found in simulations by Zapatero Osorio et al. (2002) and Palla et al. (2005) as a function of $\log g$. Another consideration is whether the observed depletion (either real or a systematic measurement error) is related to rotation rate. Studies such as Viallet & Baraffe (2012) suggest that rotationally induced mixing can deplete lithium on time-scales of just a few Myr. We observe no correlation when EW[Li] is plotted against measured $v \sin i$. The depletion we see would also conflict with the rotation rate versus CMD position correlation seen by Littlefair et al. (2011) if rotationally induced mixing were responsible.

Interpreting this trend in luminosity and EW[Li] is critically dependent on the adopted value of the convective mixing length (α). In the model where $\alpha = 1.9$, the EW[Li] trend is compatible with an evolution where ageing stars are slowly depleting lithium across the $(V - I_c)$ colour range as they contract towards the zero age main-sequence. This model agrees with Jeffries (2007) who finds a statistical decrease in radius as one moves from bright to faint objects at a given colour in the CMD. Importantly, if α is closer to 1.0 then we would expect to see a difference in dispersion with colour if a large ($\geq$10 Myr) age spread were present as at $(V - I_c) \approx 2.2$, the uncertainties on EW[Li] are less than the depletion predicted by the 10 Myr isochrone. Our data appear inconsistent with an age spread of this magnitude.

Whilst it is tempting to consider the link between EW[Li], luminosity and radius as confirmation of an age spread, it is evident from Fig. 2 that cold accretion can 'accelerate' the evolution of a star making it appear in all observable ways older. Thus, the EW[Li], luminosity and radius trends are the expected outcomes of either an age spread or cold accretion; our data do not allow us to differentiate.

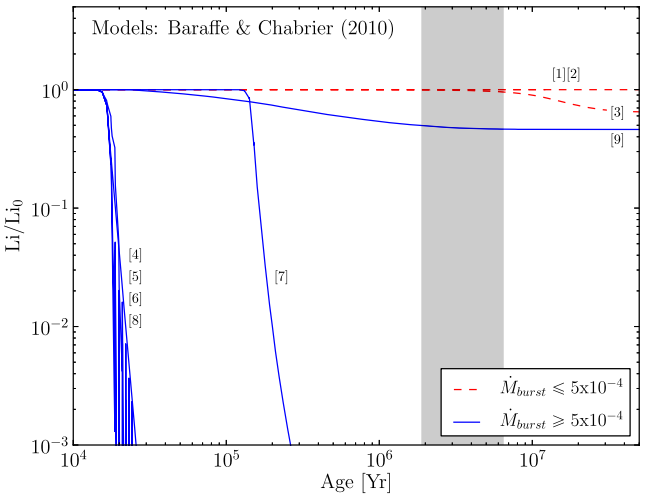

Figure 10. Evolution of the surface lithium abundance divided by initial Li abundance for a selection of models producing stars in the range $0.7 - 1\,M_\odot$ (from Baraffe & Chabrier 2010). The solid lines (blue) are those using accretion burst rates $\dot{M} = 5 \times 10^{-4}\,M_\odot\,yr^{-1}$. The dashed (red) lines are those using $\dot{M} = 1 \times 10^{-4}\,M_\odot\,yr^{-1}$. For model details see Table 3. Shaded grey region encompasses age estimates for the clusters in this study.

5.4 Depleted lithium members

It should be noted that not all cold accretion scenarios will show detectable lithium depletion in young stars in the mass ($0.3 < M_\star < 1.9\,M_\odot$) and age range ($2 - 6$ Myr) that we consider in this paper. Fig. 10 shows a range of accreting models from Baraffe & Chabrier (2010) with a selection of starting and accretion parameters that are summarized in Table 3. Our data place limits on the levels of lithium depletion seen in our sample. We observe up to $\sim$10 per cent depletion in EW[Li] which corresponds to a factor of $\lesssim$2 in lithium abundance for stars within the colour range defined by the forbidden zone. Thus, our observations exclude the possibility that our objects have experienced past accretion with $\dot{M} \geq 5 \times 10^{-4}\,M_\odot\,yr^{-1}$. The only exception might be in the case of an extremely high-mass initial core ($M_{init} > 0.03\,M_\odot$). An initial core mass $> 0.03\,M_\odot$ is at least an order of magnitude larger than expected from calculations (see

Table 3. Parameters for accreting models plotted in Fig. 10.

Reference	$M_{\rm init}$ ($M_\odot$)	$\dot{M}$ ($M_\odot yr^{-1}$)	No. of bursts	$T_{\rm quiet}$ (yr)	Time to complete accretion (yr)	Final mass ($M_\odot$)
1	0.001	1×10^{-4}	100	10^3	1.1×10^5	1.0
2	0.01	1×10^{-4}	99	10^3	1.1×10^5	1.0
3	0.01	1×10^{-4}	69	10^3	7.6×10^4	0.7
4	0.01	5×10^{-4}	14	10^3	1.5×10^4	0.7
5	0.01	5×10^{-4}	16	10^3	1.8×10^4	0.8
6	0.01	5×10^{-4}	20	10^3	2.2×10^4	1.0
7	0.01	5×10^{-4}	14	10^4	1.4×10^5	0.7
8	0.02	5×10^{-4}	20	10^3	2.2×10^4	1.0
9	0.03	5×10^{-4}	20	10^3	2.2×10^4	1.0

Baraffe et al. 2012, and references therein) of collapse from first to second Larson core (Larson 1969). Also, these high initial mass models do not explain the full range of luminosities seen in the CMD and thus do not help to explain the observed luminosity dispersion.

The lack of strongly lithium-depleted members in our sample is consistent with the findings of Palla et al. (2005) for the ONC in our mass range, and with the only available literature sample for NGC 2264 (King 1998). The Palla et al. (2005) sample has 82 stars in the ONC, in the mass range 0.4–1 $M_\odot$. Significant lithium depletion is cited for four of these stars; however (as may be seen in Fig. 7), these depleted objects are found to be broadly consistent with the spread in EW[Li] seen in our data. The levels of depletion identified are far less than we expect for cold accretion at high rates and no stars are shown to fall within the forbidden zone.

King (1998) finds that lithium abundance is indistinguishable from meteoritic values in a sample of 12 stars of spectral type range G0V–K3V in NGC 2264. The three stars closest in mass to our sample (K3V) exhibit EW[Li] ranging from 0.49 to 0.75 Å, which falls firmly within the range observed in our data.

Below the mass range that we explore, Palla et al. (2007) present lithium measurements for four objects of $M_\star < 0.3\,M_\odot$. Their EW[Li] measurements range between 0.3 and 0.44 Å, implying lithium depletion of one to two orders of magnitude, and ages of 15–30 Myr according to non-accreting models. Objects as old as this in the mass range we explore would exhibit levels of lithium far below that which we observe.

5.5 Isochronally 'old' stars

In Section 2.2, we described the selection of seven stars that appear faint with respect to the ONC cluster CMD and referred to these as the LLG. These stars could be interpreted as being older than the bulk of the population if their CMD position was considered a reliable diagnostic of age. However, four of these stars were shown in Section 4.1 to be non-members based on their RV. Of the remaining three, two lie below the 10 Myr isochrone and one lies below the 100 Myr isochrone. Whilst in CMD space these objects appear old, their measured EW[Li] and veiling ratio are entirely consistent with the other apparently younger measured stars in the cluster. If the apparently oldest star has an age that is genuinely >100 Myr, then we would expect its EW[Li] to have depleted by approximately two thirds, which we do not see. Thus, the lithium age and CMD age are in conflict. We now discuss these three stars, reconcile their photometric and EW[Li] properties and show that none are likely to be genuinely 'old' compared with the rest of the cluster.

H676. In CMD space, this star is apparently far older than the rest of the cluster with an isochronal age of >100 Myr. *Hubble Space Telescope* (*HST*) images (Smith et al. 2005) reveal an edge-on massive flared disc and accompanying Herbig–Haro jet. Its exhibited low luminosity appears to be a function of disc extinction due to the geometry of the system. It is clear from studies by Walker et al. (2004) and Mayne & Harries (2010) that circumstellar disc and accretion structures associated with young pre-MS stars can have a significant impact on the position of an object in CMD space. The disc is a clear indicator of youth and thus the age of the object should be considered consistent with its EW[Li] age of <10 Myr.

H198. This object sits below the 10 Myr isochrone in the CMD and yet has an unveiled EW[Li] of 0.57 ± 0.03 Å, which is consistent with a star that is undepleted in lithium. *HST* imagery (Bally, O'Dell & McCaughrean 2000) reveals a resolved proto-planetary disc, visible in Hα emission. It also exhibits strong evidence of interaction with a fast wind and strong UV flux from the star Θ^1 Ori C. This is evident from the strong bow shock where the T-Tauri wind interacts with the wind from the O-star. The intense UV irradiation may cause the disc to be heated, increase in thickness and photoablate (Johnstone, Hollenbach & Bally 1998). An inflated disc and downstream flow of dusty ablating material may be obscuring the central star and decreasing its apparent luminosity.

H6. This object also sits below the 10 Myr isochrone in the CMD and has an unveiled EW[Li] which is consistent with a star that is undepleted in lithium. It is found to be highly extincted in photometry by both Hillenbrand (1997) and Da Rio et al. (2009). A_V values are 3.96 and 5.30, respectively, measured at the two epochs which are separated by over a decade. Infrared colour indices $(J-H) = 1.32$ and $(J-K) = 2.12$ also indicate strong reddening, suggesting that this object is deeply embedded within its envelope or within the OMC1 molecular cloud. When subject to dereddening and extinction correction by Hillenbrand (1997), it appears that the luminosity may be underestimated. Dereddening vectors typically lie almost parallel to the pre-MS in M_V versus $(V-I_c)$ if the ratio of total to selective extinction is the typical interstellar value of $R_V \sim 3.2$ (Bessell, Castelli & Plez 1998). Mathis (1990) finds though that R_V in lines of sight through 'outer cloud dust' can be up to $R_V = 6$. A higher value of R_V increases the gradient of the reddening vector in M_V versus $(V-I_c)_0$ and leads us to infer an intrinsically brighter dereddened star than that represented in the CMD.

6 CONCLUSIONS

We have performed a spectral analysis of two young clusters, NGC 2264 and the ONC around the 6708 Å lithium doublet at a resolution of $R \sim 10\,000$. Correction has been made for accretion veiling, yielding estimates of the EW of the lithium line for 94 stars (76 single and 18 binary) in the ONC field and 74 stars (54 single and

20 binary) in the NGC 2264 field. Comparison has been made between measured EW[Li] and theory. We draw the following conclusions from our analysis.

(i) No evidence is found in 168 stars (130 unveiled stars and 38 spectroscopic binaries with lower limits) for objects with EW[Li] < 0.4 Å. This finding is consistent with that of King (1998) for 12 stars in NGC 2264 and 82 stars in the ONC of Palla et al. (2005), but we have now almost tripled the available sample. The 262 stars now observed in the two clusters place limits on cold accretion models, indicating that burst accretion rates of $\dot{M} \geq 5 \times 10^{-4}\,\mathrm{M}_{\odot}\,\mathrm{yr}^{-1}$ occur in less than 0.5 per cent of $0.3 \leq M_{\star} \leq 1.9\,\mathrm{M}_{\odot}$ stars. This mass accretion rate can only be exceeded without depleting lithium if the initial core mass is $>0.03\,\mathrm{M}_{\odot}$; however, such models seem incapable of producing the luminosity dispersion seen in CMDs. This initial core mass is also at least an order of magnitude larger than predicted by theory (see Baraffe et al. 2012, and references therein).

(ii) Approximately 10 per cent depletion in EW[Li] is seen between the brighter and fainter populations in both clusters and the depletion appears to be broadly independent of mass. This could be due to an age spread if the convective mixing length parameter (α) is close to 1.9. The scatter in age implied by the scatter in EW[Li] is similar to the small age spread implied by the scatter in CMD position. If α is closer to 1.0 then a large age spread (>10 Myr) is inconsistent with our observations and another explanation must be sought. The spread in EW[Li] is also consistent with the accelerated evolution of stellar radius and lithium abundance described by the models of past cold accretion at rates of $\dot{M} < 5 \times 10^{-4}\mathrm{M}_{\odot}\ \mathrm{yr}^{-1}$. We cannot tell which of the above scenarios are preferred as the data and models do not allow us to distinguish between the age spread and accretion mechanisms.

(iii) We targeted seven previously identified members in the ONC whose position in the CMD indicated they may be old. Four turned out to be RV non-members. The other three objects exhibit EW[Li] consistent with very young stars but are also found to be directly associated with circumstellar discs or strong extinction. Whilst in each case we cannot be sure that these features are the reason for the discrepant luminosity, it adds weight to the idea that discs and extinction contribute to the observed luminosity dispersion in pre-MS CMDs. No correlation is apparent between extinction corrected V magnitudes and derived A_V across the population as a whole.

(iv) The median accretion veiling found for single stars in the ONC ($r_j = 0.24$) is greater than that seen in NGC 2264 ($r_j = 0.13$). In addition, the ONC displays nine highly veiled objects ($r_j > 1$) whereas none are seen in NGC 2264. The highest veiling ratio seen in the ONC is 4.0 and in NGC 2264 is 1.0.

(v) When establishing membership lists for young clusters (<10 Myr), lithium detection is a necessary requisite for membership confirmation in the mass range $0.3 \leq M_{\star} \leq 1.9\,\mathrm{M}_{\odot}$. If lithium is not detected, a star must have less than 0.5 per cent chance of being a young cluster star.

ACKNOWLEDGEMENTS

DJS is funded by a UK Science and Technology Facilities Council (STFC) studentship. The authors wish to thank Isabelle Baraffe for providing cold accretion models and useful discussions. Spectra were extracted and calibrated using the AF2 pipeline developed by Richard Jackson. This research is based on observations made with the *William Herschel* Telescope operated on the island of La Palma by the *Isaac Newton* Group (ING) in the Spanish Observatorio del Roque de los Muchachos of the Instituto de Astrofisica de Canarias. This research has made use of archival data products from the Two-Micron All-Sky Survey (2MASS), which is a joint project of the University of Massachusetts and the Infrared Processing and Analysis Center, funded by the National Aeronautics and Space Administration (NASA) and the National Science Foundation.

REFERENCES

Anders E., Grevesse N., 1989, Geochim. Cosmochim. Acta, 53, 197
Ballesteros-Paredes J., Hartmann L., 2007, Rev. Mex. Astron. Astrofis., 43, 123
Bally J., O'Dell C. R., McCaughrean M. J., 2000, AJ, 119, 2919
Baraffe I., Chabrier G., 2010, A&A, 521, A44
Baraffe I., Chabrier G., Allard F., Hauschildt P. H., 2002, A&A, 382, 563
Baraffe I., Chabrier G., Gallardo J., 2009, ApJ, 702, L27
Baraffe I., Vorobyov E., Chabrier G., 2012, ApJ, 756, 118
Baxter E. J., Covey K. R., Muench A. A., Fűrész G., Rebull L., Szentgyorgyi A. H., 2009, AJ, 138, 963
Bell C. P. M., Naylor T., Mayne N. J., Jeffries R. D., Littlefair S. P., 2013, MNRAS, in press
Bessell M. S., Castelli F., Plez B., 1998, A&A, 333, 231
Biazzo K., Melo C. H. F., Pasquini L., Randich S., Bouvier J., Delfosse X., 2009, A&A, 508, 1301
Carlsson M., Rutten R. J., Bruls J. H. M. J., Shchukina N. G., 1994, A&A, 288, 860
Da Rio N., Robberto M., Soderblom D. R., Panagia N., Hillenbrand L. A., Palla F., Stassun K., 2009, ApJS, 183, 261
Da Rio N., Gouliermis D. A., Gennaro M., 2010, ApJ, 723, 166
Dahm S. E., Simon T., 2005, AJ, 129, 829
Dodin A. V., Lamzin S. A., 2012, Astron. Lett., 38, 649
Elmegreen B. G., 2000, ApJ, 530, 277
Enoch M. L., Evans N. J., II, Sargent A. I., Glenn J., 2009, ApJ, 692, 973
Flaccomio E., Micela G., Sciortino S., Favata F., Corbally C., Tomaney A., 1999, A&A, 345, 521
Flaccomio E., Damiani F., Micela G., Sciortino S., Harnden F. R., Jr, Murray S. S., Wolk S. J., 2002, in Favata F., Drake J. J., eds, ASP Conf. Ser. Vol. 277, Chandra X-ray Observation of the Orion Nebula Cluster. Astron. Soc. Pac., San Francisco, p. 155
Fűrész G. et al., 2006, ApJ, 648, 1090
Fűrész G., Hartmann L. W., Megeath S. T., Szentgyorgyi A. H., Hamden E. T., 2008, ApJ, 676, 1109
Gahm G. F., Walter F. M., Stempels H. C., Petrov P. P., Herczeg G. J., 2008, A&A, 482, L35
Guenther E., Hessman F. V., 1994, in The P. S., Perez M. R., van den Heuvel E. P. J., eds, ASP Conf. Ser. Vol. 62, The Veiling Continuum of T Tauri stars. Astron. Soc. Pac., San Francisco, p. 132
Hartigan P., Hartmann L., Kenyon S., Hewett R., Stauffer J., 1989, ApJS, 70, 899
Hartmann L., Cassen P., Kenyon S. J., 1997, ApJ, 475, 770
Hartmann L., Zhu Z., Calvet N., 2011, preprint (arXiv:1106.3343)
Herbst W., Bailer-Jones C. A. L., Mundt R., Meisenheimer K., Wackermann R., 2002, A&A, 396, 513
Hillenbrand L. A., 1997, AJ, 113, 1733
Horne K., 1986, PASP, 98, 609
Hosokawa T., Offner S. S. R., Krumholz M. R., 2011, ApJ, 738, 140
Jeffries R. D., 2007, MNRAS, 381, 1169
Jeffries R. D., Oliveira J. M., 2005, MNRAS, 358, 13
Jeffries R. D., Oliveira J. M., Barrado y Navascués D., Stauffer J. R., 2003, MNRAS, 343, 1271
Jeffries R. D., Littlefair S. P., Naylor T., Mayne N. J., 2011, MNRAS, 418, 1948
Johnstone D., Hollenbach D., Bally J., 1998, ApJ, 499, 758
Kenyon S. J., Hartmann L., 1995, ApJS, 101, 117
Kenyon S. J., Hartmann L. W., Strom K. M., Strom S. E., 1990, AJ, 99, 869
King J. R., 1998, AJ, 116, 254

Lamm M. H., Bailer-Jones C. A. L., Mundt R., Herbst W., Scholz A., 2004, A&A, 417, 557
Larson R. B., 1969, MNRAS, 145, 271
Littlefair S. P., Naylor T., Mayne N. J., Saunders E., Jeffries R. D., 2011, MNRAS, 413, L56
Mathis J. S., 1990, in Blitz L., ed., ASP Conf. Ser. Vol. 12, Interstellar Dust and Extinction. Astro. Soc. Pac., San Francisco, p. 63
Mayne N. J., Harries T. J., 2010, MNRAS, 409, 1307
Mayne N. J., Naylor T., 2008, MNRAS, 386, 261
Mayne N. J., Naylor T., Littlefair S. P., Saunders E. S., Jeffries R. D., 2007, MNRAS, 375, 1220
McNamara B. J., 1976, AJ, 81, 845
Menten K. M., Reid M. J., Forbrich J., Brunthaler A., 2007, A&A, 474, 515
Naylor T., 2009, MNRAS, 399, 432
Palla F., Stahler S. W., 2000, ApJ, 540, 255
Palla F., Randich S., Flaccomio E., Pallavicini R., 2005, ApJ, 626, L49
Palla F., Randich S., Pavlenko Y. V., Flaccomio E., Pallavicini R., 2007, ApJ, 659, L41
Pflamm-Altenburg J., Kroupa P., 2007, MNRAS, 375, 855
Pinsonneault M., 1997, ARA&A, 35, 557
Rhode K. L., Herbst W., Mathieu R. D., 2001, AJ, 122, 3258
Sacco G. G., Randich S., Franciosini E., Pallavicini R., Palla F., 2007, A&A, 462, L23
Siess L., Dufour E., Forestini M., 2000, A&A, 358, 593
Smith N., Bally J., Licht D., Walawender J., 2005, AJ, 129, 382
Tan J. C., Krumholz M. R., McKee C. F., 2006, ApJ, 641, L121
Tout C. A., Livio M., Bonnell I. A., 1999, MNRAS, 310, 360
van Hamme W., 1993, AJ, 106, 2096
Viallet M., Baraffe I., 2012, A&A, 546A, 113
Vorobyov E. I., Basu S., 2005, ApJ, 633, L137
Walker C., Wood K., Lada C. J., Robitaille T., Bjorkman J. E., Whitney B., 2004, MNRAS, 351, 607
Zapatero Osorio M. R., Béjar V. J. S., Pavlenko Y., Rebolo R., Allende Prieto C., Martín E. L., García López R. J., 2002, A&A, 384, 937

SUPPORTING INFORMATION

Additional Supporting Information may be found in the online version of this article:

Table 2. Summary of derived parameters from this study. Table 2 is published in its entirety in the electronic edition. A portion is shown here for guidance regarding its form and content. Coordinates are RA, Dec. (J2000.0). Importantly, the resolution and sky subtraction scheme used in this analysis mean that nebular line contamination of Hα measurements is likely to be significant and thus Hα data should be used with caution. EW[Hα] measurements are not corrected for veiling. (http://mnras.oxfordjournals.org/lookup/suppl/doi:10.1093/mnras/stt973/-/DC1).

Please note: Oxford University Press are not responsible for the content or functionality of any supporting materials supplied by the authors. Any queries (other than missing material) should be directed to the corresponding author for the article.

This paper has been typeset from a TEX/LATEX file prepared by the author.